Interactive learning of implicative fuzzy rules applied to the classification of POLSAR features in the context of Alpine glaciers

Gabriel Vasile, Lavinia Darlea, Sylvie Galichet, Lionel Valet, Emmanuel Trouvé, Ivan Petillot, Michel Gay

Gabriel Vasile, Lavinia Darlea, Sylvie Galichet, Lionel Valet, Emmanuel Trouvé, et al.. Interactive learning of implicative fuzzy rules applied to the classification of POLSAR features in the context of Alpine glaciers. [Research Report] GIPSA-LAB. 2007. hal-01402251

HAL Id: hal-01402251
https://hal.science/hal-01402251v1

Submitted on 24 Nov 2016

Interactive learning of implicative fuzzy rules applied to the classification of POLSAR features in the context of Alpine glaciers

Gabriel VASILE(1), Lavinia DARLEA(2,3), Sylvie GALICHET(2), Lionel VALET(2),
Emmanuel TROUVÉ(2), Ivan PÉTILLOT(2) and Michel GAY(1)

(1): Laboratoire Grenoble Images Parole Signal Automatique, GIPSA-lab / CNRS
BP 46 - 38402 Saint-Martin-d'Hères - FRANCE
Tel: +33 476 826 260 - Fax: +33 476 826 384 - Email: michel.gay@gipsa-lab.inpg.fr

(2): Laboratoire d'Informatique, Systèmes, Traitement de l'Information et de la Connaissance
Université de Savoie - BP 806 - 74016 Annecy Cedex - FRANCE - Tel: +33 450 096 548 - Fax: +33 450 096 559
Email: {g.vasile|lavinia.darlea|lionel.valet|sylvie.galichet|trouve|ivan.petillot}@univ-savoie.fr

(3): Laboratorul de Analiza si Prelucrarea Imaginilor, Universitatea POLITEHNICA Bucuresti
24, Bd. Iuliu Maniu, Nr. 1-3, Bucharest - ROMANIA
Tel/Fax : +4021 402 4683 - Email: {gvasile|ldarlea}@alpha.imag.pub.ro

ABSTRACT

With the developments of airborne, and recently spaceborne, fully polarimetric synthetic aperture radar (POLSAR) sensors, microwave remote sensing offers new opportunity to observe and understand geophysical phenomena. However, extracting information from the multi-component complex POLSAR images requires several processing stages, including the POLSAR feature estimation to reveal different backscattering mechanisms, and the fusion of these features to help the end-user to perform detection or classification tasks. In this paper, a new data fusion method based on interactive learning of implicative fuzzy rules is presented. It allows to perform supervised classification by analyzing the training set clusters in the different 2D feature spaces resulting from the different attribute pairs. Experimental results are presented on a real POLSAR data set acquired by the airborne E-SAR system over temperate glaciers in the Alps. They illustrate the interest of the proposed fusion approach for POLSAR data analysis and the potential of the POLSAR imagery for the monitoring of temperate glacier evolution.

Contents

1 Introduction

The Alpine glacier activity has been observed by ground measurements since the end of the 19^{th} century [1]. In the last decades, understanding and monitoring their evolution have become important issues for several reasons including geophysical hazard and water resource assessment, economical activity in the surrounding areas and scientific investigations regarding the local effects of global warming. Located in mountainous areas, most of the Alpine glaciers are difficult and dangerous to access. In this environment, ground measurements are performed only on some glaciers, on a few points, and usually only once a year during the warmest season. Remote sensing offers the opportunity to strongly increase glacier spatial and temporal observations, especially through optical and radar sensors [2], [3], [4], [5], [6]. The use of optical high resolution images allows the measurement of the surface topography and velocity at summer time [7]. However, the availability of these images is constrained by meteorological conditions and the snow cover makes such measurements impossible.

With all weather capabilities, Synthetic Aperture Radar (SAR) images are a regular source of information which may provide different measurements based on the radar specificity: snow and ice penetration which yields to subsurface observation, coherent waves which allow interferometric applications, and polarized waves which allow the analysis of the backscattering media. However, interferometric or polarimetric SAR acquisitions provide multichannel complex images which require a heavy processing chain, especially in the context of Alpine glaciers with high relief, fast motion and surface changes and a rather unknown SAR signature of the ice/snow/rock mixture. The processing chain can be divided into two main stages:

- an information extraction stage to obtain higher level information than the initial SAR data. This stage can be performed by conventional methods now available in distributed software programmes [8].
- an information fusion stage which can be performed by different approaches depending on the application requirements. In this paper, we propose a novel supervised classification approach based on a two by two analysis of attributes extracted from polarimetric SAR images acquired over Alpine glaciers.

Basically, SAR systems measure both amplitude and phase of the backscattered signal, producing one complex image for each recording. Polarimetric synthetic aperture radar (POLSAR) is an extension of the SAR imaging system, the sensors being able to emit and receive two polarizations, usually horizontal (H) and vertical (V). Four polarization configurations, usually denoted by HH, VV, HV and VH (according to the emitted and received polarization) are simultaneously available. Under the assumption of reciprocal symmetric backscattering, the HV and VH modes are fused and the resulting configuration is denoted by XX. Polarimetric monostatic acquisitions are usually represented in the Pauli basis and are fully described by the 3×3 polarimetric coherency matrix [9].

The information provided by SAR polarimetry allows the discrimination of different scattering mechanisms. The first characteristic decomposition of target coherency matrix for target scattering decomposition was proposed in [10]. The received signal can be split into a sum of three scattering contributions with orthogonal polarimetric signatures. The orthonormal eigenvectors of the Hermitian target coherency matrix are used to analyze the eigenvector space.

The dominant scattering mechanism is represented by the largest eigenvalue of the coherency matrix. In [9], Cloude and Pottier introduced the target entropy H and the $\alpha - \beta$ model by assigning the corresponding coherent single scattering mechanism to each eigenvector. Other polarimetric decompositions have been proposed: Huynen [11], Barnes [12] (non-coherent), Krogager [13], Cameron [14] (coherent) or Freeman [15] (model-based). In [16], Ridha Touzi proposed a unified roll-invariant decomposition of coherent and partially coherent target scattering. These decomposition techniques provide useful attributes for classification.

In the literature, many classification algorithms for POLSAR data have been proposed. A state of the art can be found in [17] and [18]. Basically, three general approaches can be identified: analysis of physical scattering properties [19], [9], statistical clustering [20], [21], [22] and combined physical/statistical classification [23], [24], [25], [26]. These algorithms can be either supervised or unsupervised and each of the two strategies having its own advantages and disadvantages, depending on the application field, the availability of ground truth and the level of expertise of the users. For example, Lee et al. proposed in [23] a combination of unsupervised classification based on Cloude and Pottier polarimetric decomposition [9] and the maximum likelihood classifier based on the complex Wishart distribution of the polarimetric covariance matrix. This approach was extended for coherence matrices [24] and for Freeman and Durden decomposition [25].

In [26], Kersten et al. proposed an interesting study in which five statistical clustering techniques were compared by classifying a POLSAR image. The general procedure recommended for unsupervised POLSAR classification is described by the following processing chain [26]:

1. speckle filtering, necessary for robust polarimetric parameter estimation and for avoiding over-segmentation,
2. Cloude and Pottier decomposition and unsupervised H-α classification,
3. refined fuzzy c-mean clustering of the logarithm of the covariance matrix diagonal terms using the ℓ_2 norm,
4. checking the numerical stability of the data,
5. refined fuzzy c-mean clustering based on the Bartlett dissimilarity measure,
6. Wishart or expectation-maximum clustering.

The final conclusion of this study is that, for POLSAR classification, it is essential to model correctly the pixel distribution and its associated dissimilarity measures, the statistical clustering mechanism itself being less important.

In this paper, a different fusion approach is proposed to perform a supervised classification of POLSAR attributes. This approach consists in learning implicative fuzzy rules that define the sought-after classes in the feature space. These specific rules are learnt from convex polygons which match the positive examples in the different 2D feature spaces corresponding to the different possible pairs of attributes. Compared to conventional supervised classifiers such as neural networks (NN) or support vector machines (SVM), the proposed method offers the advantage of being close to the end-user reasoning and the conventional POLSAR feature analysis performed for instance in the entropy-alpha, entropy-anisotropy and anisotropy-alpha spaces [9]. These 2D analysis often consist in crisp partitioning of the 2D feature spaces followed by a statistical Wishart classifier which refine the clustering according to "electromagnetic backscattering" information brought by coherency matrices. With a different approach, the proposed method investigates the 2D feature spaces according to the training set and yields two different results:

- a classification which corresponds to a clustering based on the geophysical information provided through the learning set and includes mixed-classes for overlapping behaviors,
- the associated description of the classes in the different pairs of attributes which allows the end-user to interpret the results and the polarimetric characteristics of the different classes.

The remainder of this paper is organized as follows. In Section II, the principles of the conventional POLSAR attribute extraction are briefly reviewed. Section III is dedicated to the presentation of the proposed implicative fuzzy rules (IFR) fusion method and its application in the case of multi-class multi-attribute classification. In Section IV, experimental results are presented on POLSAR features extracted from a polarimetric SAR data set acquired by the German E-SAR airborne sensor [27] over Alpine glaciers located in the Mont-Blanc area. The principle and the behaviour of the proposed method are illustrated by entropy-alpha-anisotropy classification performed to investigate the POLSAR characteristics of a well-known phenomenon: the Forbes bands [28]. Eventually, in Section V, some conclusions and perspectives are presented.

2 POLSAR information extraction

The first stage of a processing chain dedicated to the classification of POLSAR data usually consists in extracting polarimetric features which provide higher level information than the initial complex multi-channel SAR images. In this section, the main steps of this "information extraction" stage are recalled and the conventional features used as attributes in the fusion stage are described.

The initial polarimetric SAR acquisition performed in a monostatic configuration (emitting and receiving antenna located in almost the same place) results in a 3-channel complex image, each channel corresponding to a different polarisation configuration, usually denoted by S_{HH}, S_{VV}, S_{XX}. The Pauli basis [29] is usually preferred to obtain a coherent scattering vector $[k]$ closer to the physical phenomena of wave scattering:

$$[k] = \frac{1}{\sqrt{2}} \begin{bmatrix} S_{HH} + S_{VV} \\ S_{HH} - S_{VV} \\ 2S_{XX} \end{bmatrix}. \tag{1}$$

Except for a coherent target, the speckle phenomenon which affects the distributed targets makes it difficult to work directly with the scattering vectors. A second order representation of the data is usually obtained by estimating the 3×3 Hermitian positive semidefinite coherency matrix:

$$[T] = E\{[k][k]^{*t}\} \tag{2}$$

where $E\{...\}$ denotes the expectation value. Under stationarity and ergodicity assumptions, the coherency matrix can be estimated by the spatial sample averaging. Several techniques have been proposed to estimate the coherency matrix using adaptive neighborhoods and/or adaptive estimators [30].

These coherency matrices follow Complex Wishart distributions which can be used to build statistical classifiers such as the maximum likelihood. However, it is usually difficult to perform a direct interpretation of these 3×3 coherency matrices in terms of backscattering mechanism of geophysical information. In [9], Cloude and Pottier proposed a decomposition based on the projection of the polarimetric coherency matrix $[T]$ onto its eigenvalues basis. The matrix $[T]$ is given by a weighted sum of three unitary matrices of rank one, each representing a pure scattering mechanism $[T^{(i)}]$:

$$[T] = \sum_{i=1}^{3} \lambda_i [v]_i [v]_i^{*T} = \sum_{i=1}^{3} \lambda_i [T^{(i)}], \tag{3}$$

where $\lambda_1 > \lambda_2 > \lambda_3$ are the ordered eigenvalues and v_i their corresponding eigenvectors. The entropy H and anisotropy A have been defined as:

$$H = \sum_{i=1}^{3} -P_i log_3 P_i, \tag{4}$$

$$A = \frac{\lambda_2 - \lambda_3}{\lambda_2 + \lambda_3}, \tag{5}$$

where the pseudo-probabilities P_i are given by:

$$P_i = \frac{\lambda_i}{\sum_{j=1}^{3} \lambda_j}. \tag{6}$$

Also the α parameter is given as the weighted mean of the α_i parameters corresponding to the three scattering mechanisms [9]:

$$\alpha = \sum_{i=1}^{3} P_i \alpha_i. \tag{7}$$

The extracted meaningful roll-invariant parameters H, A and α indicate the random behavior of the global scattering and the mean scattering mechanism from surface to double bounce scattering. They are strongly related to the geophysical properties of the ground target area providing reliable information for further classification. In [9], nine clustering zones are proposed to describe the H and α plane. The boundaries of such crisp predefined clustering (see Fig. 8) are often used as references to interpret the attribute spaces in terms of backscattering mechanisms. However, used as a classification method or to initialize unsupervised classifiers, these clusterings are not always appropriate to obtain a thematic classification related to the ground cover. The main difficulties come either from the POLSAR feature extraction which cannot avoid estimation bias and variances, or from the “thematic classes” corresponding to clusters which spread in the different 2D feature spaces over several “backscattering clusters”.

3 Information fusion

This section is dedicated to the second stage of the information processing chain, namely ”information fusion”. The objective is to merge different information sources (POLSAR attributes) for constructing the classification map. Moreover, our goal is also to provide the end-user with a description of the sought-after classes, by means of implicative fuzzy rules.

3.1 One-class binary classifiers

Let us first consider a one-class binary classification problem of assigning a class label $l \in \{P, N\}$ to the input feature vector x composed of two attributes, i.e. $x = (x_1, x_2)$. In other words, the label P corresponds to positive examples belonging to the class under consideration and the class label N to negative examples situated outside of the sought-after class.

For single-class classification, we focus in this paper on Positive Example Based Learning, referred as PEBL in [31]. The learning task consists in finding a mapping $f : R^2 \mapsto \{ P, N\}$ that "best" represents a training set of positive examples. So that this learning may become possible, the function space from which f is to be selected must be defined. We propose to use a specific class of fuzzy systems, based on implicative fuzzy rules or gradual rules. This allows the specification of f by a collection of linear inequalities involving the x_1 and x_2 features. This representation is completely equivalent to defining the class boundary in the 2D feature space by a convex polygon.

Most studies concerning the use of fuzzy rules for classification problems [32], [33], [34], [35] are based on a conventional expression of the rules in a multi-class framework with a n-dimensional feature space, such as: "**If** x_1 **is** F_1 **and ... and** x_n **is** F_n **then class is** C_k". In general, the fuzzy aggregation operators, which are used either for directly implementing the rules or for weighting them by a certitude degree, suppose both a disjunctive combination of these rules (mostly the "max" operator) and a conjunctive interpretation of the "**If ... then ...**" logical operator. The proposed classification approach lies in the same methodological context, but introduces a particular form for the rule premise which allows class modeling by means of gradual rules [36], [37].

The implementation of gradual rules usually expressed as "**The more** x_1 **is** F_1**, the more** x_2 **is** F_2" is based on the use of an implicative operator, which means that gradual rules can be viewed as special cases of "**If** x_1 **is** F_1 **then** x_2 **is** F_2" rules. Actually, the gradual semantics is due to the choice of a residuated fuzzy implication. In the remaining part of this paper, the Rescher-Gaines implication is assumed:

$$a \to b = 1 \text{ if } a \leq b, \tag{8}$$

$$a \to b = 0 \text{ if } a > b, \tag{9}$$

where $a, b \in [0, 1]$ are truth values. In this case, an appropriate adjustment of the fuzzy subsets F_1 and F_2 results in the construction of a binary graph that linearly separates the feature space into two-half planes (see the red rectangle in Fig. 1). In this framework, the purpose of this section is:

1. discussing some reasonable conditions on the involved fuzzy subsets that result in a linear separation in the feature space,
2. proposing an algorithm that builds a gradual rule and tunes all its elements for an exact representation of a given linear constraint,

3. learning from positive examples a collection of gradual rules that models a convex polygon-shaped class.

Generally speaking, the graph corresponding to the gradual rule "**If** x_1 **is** F_1 **then** x_2 **is** F_2" can be defined as:

$$\Gamma(x_1, x_2) = \mu_{F_1}(x_1) \rightarrow \mu_{F_2}(x_2), \tag{10}$$

where $\mu_{F_i}(x_i)$, $i \in \{1, 2\}$ represents the membership degree of x_i in the fuzzy subset F_i.

[Figure 1 about here.]

Considering bounded universes of discourse for each attribute, $X_1 = [x_{1min}, x_{1max}]$ and $X_2 = [x_{2min}, x_{2max}]$, and defining the membership functions of F_1 and F_2 as increasing or decreasing ramps bounded by 0 and 1 [Fig 1], this leads to a feasible characterization of the graph Γ. Indeed, solving the equation $\mu_{F_1}(x_1) = \mu_{F_2}(x_2)$ on the cartesian product $X_1 \times X_2$ results in solving a linear equation that constitutes the boundary between points that belong to the graph, i.e. *positive examples*, and points that do not, i.e. *negative examples*.

For example, in the case of Fig 1, we have $X_1 = [x_{1min}, x_{1max}] = [1, 3.5]$ and $X_2 = [x_{2min}, x_{2max}] = [1, 4]$. The membership function of F_1 is defined as:

$$\mu_{F_1}(x_1) = \begin{cases} 0 & \text{if } x_1 < 1, \\ 0.4(x_1 - 1) & \text{if } x_1 < 3.5, \\ 1 & \text{otherwise.} \end{cases} \tag{11}$$

For the fuzzy subset F_2, we have:

$$\mu_{F_2}(x_2) = \begin{cases} 1 & \text{if } x_2 < -1, \\ -0.2x_2 + 0.8 & \text{if } x_2 < 4, \\ 0 & \text{otherwise.} \end{cases} \tag{12}$$

On $X_1 \times X_2$, it follows that $\mu_{F_1}(x_1) = \mu_{F_2}(x_2)$ if and only if $2x_1 + x_2 - 6 = 0$. Finally, according to Eqs. 8 and 9, $\Gamma(x_1, x_2) = 1$ if $2x_1 + x_2 - 6 \leq 0$ and $\Gamma(x_1, x_2) = 0$ in the opposite case. It means that the implicative fuzzy rule "**If** x_1 **is** F_1 **then** x_2 **is** F_2" implements a linear constraint on $X_1 \times X_2$ and can thus be used as a linear discriminant. It is worth noting that the graph extension induced by the natural extension of the membership function of F_2 outside of X_2 does not result in the propagation of the linear constraint defined on the subspace $X_1 \times X_2$ (dark blue graph in Fig. 1). It means that a particular attention has to be paid to the closure of the constrained space.

Let us also mention that fuzzy graphs can be obtained either by refining the rule-based representation as discussed in [37] or by choosing a more sophisticated residuated implication operator. Such an enhanced handling of fuzzy gradual rules is however not considered here.

The integration of gradual rules into classification systems requires their transformation into usual classification rules expressed as fuzzy "**If** ... **then** ..." rules the conclusions of which only involve class labels. It means that any attribute that appears in the conclusion part of a gradual rule has to be transferred into the premise part of an equivalent classification rule. The implicative operator implicitly assumed when implementing gradual rules has also to be transferred into the rule premise in order to preserve the desired semantics. It has been proved in [38] that an exact equivalence between both formalisms can be achieved by transforming the implicative rule "**If** x_1 **is**

F_1 **then** x_2 **is** F_2" into the classification rule "**If** x_1 *is* $F1 \ \rightarrow\ x_2$ *is* F_2 **then class is** P". By doing so, the "shape" of the graph associated with the gradual rule is encapsulated in the premise part of the rule the conclusion of which now specifies that the feature vector is a positive example of the class under consideration. Thus, except the implication based computation of the rule firing degree, the classification rule implementation is quite usual: a conjunctive interpretation of the "**If** ... **then** ..." operator is assumed.

Let us now present the automatic generation of a gradual rule (the implication-based antecedent of a classification rule), for exactly representing a linear constraint given by the inequality $ax_1 + bx_2 + c \leq 0$ in the bounded subspace $X_1 \times X_2 = [x_{1min}, x_{1max}] \times [x_{2min}, x_{2max}]$. In other words, we have to determine the membership function of F_1 and F_2 so that $\mu_{F_1}(x_1) \rightarrow \mu_{F_2}(x_2) = 1$ whenever $ax_1 + bx_2 + c \leq 0$. According to the above study, it appears that a solution consists in restricting the problem to the use of ramp-shaped membership functions as illustrated in Fig. 2. In this context, a fuzzy subset F defined on the universe of discourse X is represented by three parameters, i.e. $F \equiv (f_{min}, f_{max}, t)$ where $[f_{min}, f_{max}] \subset X$ is the interval on which the membership degree linearly varies between 0 and 1. The third parameter $t \in \{\nearrow, \searrow\}$ is interpreted as the evolution tendency of the membership function on $[f_{min}, f_{max}]$, i.e increasing or decreasing.

[Figure 2 about here.]

In the so-defined context, the algorithm given below provides us with a simple method for generating automatically the fuzzy subsets F_1 and F_2 so that the rule "**If** x_1 *is* $F_1 \ \rightarrow\ x_2$ *is* F_2 **then class is** P" represents positive examples which satisfy a known linear constraint.

Algorithm 1

```
Inputs:
- $X_1 \times X_2 = [x_{1min}, x_{1max}] \times [x_{2min}, x_{2max}]$ the rectangle-shaped working subspace
- $ax_1 + bx_2 + c \leq 0$, the constraint to be implemented by the fuzzy rule.
Outputs:
- Fuzzy subsets $F_1$ and $F_2$ to be used in the rule "If $x_1$ is $F_1 \rightarrow x_2$ is $F_2$ then class is $P$".

Find the two points where the straight line $ax_1 + bx_2 + c = 0$ intersects the rectangular boundary of the
working space $X_1 \times X_2$, that is $(x_1^{(1)}, x_2^{(1)})$ and $(x_1^{(2)}, x_2^{(2)})$;

if $a \leq 0$ then $F_1 \equiv [\min(x_1^{(1)}, x_1^{(2)}),\ \max(x_1^{(1)}, x_1^{(2)}), \searrow]$;
else $F_1 \equiv [\min(x_1^{(1)}, x_1^{(2)}),\ \max(x_1^{(1)}, x_1^{(2)}), \nearrow]$;
endif;

if $b \leq 0$ then $F_2 \equiv [\min(x_2^{(1)}, x_2^{(2)}),\ \max(x_2^{(1)}, x_2^{(2)}), \nearrow]$;
else $F_2 \equiv [\min(x_2^{(1)}, x_2^{(2)}),\ \max(x_2^{(1)}, x_2^{(2)}), \searrow]$;
endif.
```

Dealing with several linear constraints is immediate: we just have to specify that all the constraints have to be satisfied at the same time for an example to be positive. It follows that the rule premise is defined as the conjunction of all constraints, or equivalently as the conjunction of all implicative relations. Handling n constraints thus leads to rules of the form:

$$\text{"}\textbf{If } (x_1 \textbf{ is } F_1^{(1)} \rightarrow x_2 \textbf{ is } F_2^{(1)}) \textbf{ and } (x_1 \textbf{ is } F_1^{(2)} \rightarrow x_2 \textbf{ is } F_2^{(2)}) \ldots \textbf{ and } (x_1 \textbf{ is } F_1^{(n)} \rightarrow x_2 \textbf{ is } F_2^{(n)}) \textbf{ then class is } P\text{"}, \tag{13}$$

where the pair of fuzzy subsets $(F_1(i), F_2(i))$, $i \in \{1, ...n\}$, built using the above algorithm, represents the i^{th} constraint. The synthesis of such a rule for 6 constraints, representing a 6-side polygon, is detailed in Fig. 3, in which the closed domain $[-0.5, 0.75] \times [-0.7, 1]$ is assumed. The four possible tendencies concerning the pairs (F_1, F_2) are illustrated with the constraints $C1$, $C2$, $C3$ and $C5$ (right hand side of Fig. 3). The implication-based representation of the two other constraints, i.e. $C4$ and $C6$ which respectively define the horizontal and vertical polygon boundaries, leads to unit step membership functions either for F_2 or for F_1.

[Figure 3 about here.]

Let us finally come back to the initial problem of learning a binary one-class classifier from positive examples. In the assumed context of convex polygon-shaped classes, the "best" polygon for representing the class under consideration has to be determined. This task viewed as the process of extracting constraints from data has to be achieved prior to rule synthesis. Later on, in Sect. 4, a conventional algorithm able to compute the convex hull of 2D data will be used for this purpose in two different ways. The first one consists in considering all available positive examples to determine the polygonal shape of the class. The second approach includes a data pre-processing step in charge of refining the set of positive examples before the convex hull extraction.

3.2 Multi-attribute, multi-class classification

The rule-based technique presented in the previous section was clearly designed for implementing binary classifiers in a 2D feature space. In practice, it is required that the proposed methodology be embedded into a more general classification scheme suitable for:

- multi-attribute fusion,
- multi-class decision.

Both points are dealt with independently in the chosen two-level architecture presented in Fig. 4. The first level, focusing on the attribute fusion process, is thus tackled in the framework of the one-class binary classification. It means that a multi-attribute classifier is built for each class. The latter computes a class score which is then combined with other class scores in the second level in charge of the final decision. Both fusion processes are briefly described in the remaining part of this section.

Assuming gradual rule based classification, the restriction on the number of fused attributes is mainly due to the use of an implicative operator, neither commutative nor associative by nature. Obviously this important drawback has to be countered to make the method applicable to practical classification problems. We propose here to address the multi-attribute fusion by taking all possible pairs of attributes for the class assignment into account. Working in a p-dimensional feature space, a collection of $C = p(p-1)/2$ classifiers are thus developed. Each of them provides a partial own-viewed decision concerning the belonging (positive labeling) to the class under consideration. All attribute pairs are then viewed as voting for or against the assignment of the feature vector to the studied class. Every positive vote is counted by the aggregation operator A_{vote} in Fig. 4 that finally computes the class score as the percentage of positive votes with respect to the total number of votes C.

[Figure 4 about here.]

At the second fusion stage, the final decision is achieved by the aggregation procedure A_{class} according to the following policy:

- When all the sought-after classes get scores strictly below 50%, the feature vector is not assigned to any of them (simple majority requirement). Actually, unclassified examples are grouped into an additional class (reject class).
- Classes succeeding with the majority requirement become admissible candidates for the feature vector assignment. When several classes are eligible for the final decision, the one with the maximum score is selected.
- If the maximum score is achieved by several classes simultaneously, the point is classified into a new class that represents the ambiguity between involved classes.

4 Results and discussion

To illustrate the performances of the proposed method, results obtained with real airborne polarimetric SAR images are reported.

4.1 Experimental data

A collaboration between the German Aerospace Center (DLR) and 4 French laboratories has been initiated to acquire airborne high resolution POLSAR data over several Alpine glaciers from the "Chamonix Mont-Blanc" (France) test site [27]. Two multi-polarization data set have been collected in October 2006 and February 2007 by the DLR's airborne Experimental Synthetic Aperture Radar System (E-SAR) in order to analyse the SAR backscattering properties of temperate glacier. The data set used in this paper represents a fully polarimetric L-band monostatic acquisition (parameters reported in Tab. 1) over the Tacul glacier, one of the three glaciers forming the second glacial complex in Europe after Aletsch (Switzerland), namely Mer-de-glace [39].

[Table 1 about here.]

One of the particularities of the Tacul glacier is the presence of the Forbes bands phenomenon [28]: the alternation of white and dark bands whose shape looks like diagonal arches [Fig. 5-(b)]. The cause of this phenomenon still raises many debates in the glaciological community. One generally accepted explanation lies in the fact that more ice slides down in summer than in winter. The surface of the ice below the Géant icefall (upper part of the Tacul glacier) forms a series of terraces. The slopes of the terraces which have a northern orientation melt less than those oriented southwards, the former exhibiting also purer ice than the latter [40]. This alternation of clean and dirty ice is due to the variation in the quantity of mineral dust (cryoconites) [41].

Recently, Guy at al. proposed to interpret the cryoconite origin by the influence of the content of mineral matter on the lowering of the temperature and pressure of ice fusion and upon the increase of fusion velocity [42], [41]. Basically, the dust grains which are incorporated in the ice are surrounded by a film of liquid water (tenth of microns for micron roughness) and this induces the local lowering of the fusion temperature of about $1^0 C$. One conclusion of the study presented in [42] is that dirty (summer) ice melts faster than clean (winter) ice.

At first, the Forbes bands run pretty much across the glacier, but as afterwards their center moves more rapidly than the sides, they acquire farther down a curved shape, as it can be observed in the optical image from Fig. 5-(b). Their curvature shows the varying velocity of the ice advances in the different parts of its course, being one good indicator of the differential in flow speed [40].

[Figure 5 about here.]

The Single Look Complex (SLC) test images have 1205 × 1312 pixels each. After initial 4-look complex multi-looking, the IDAN speckle filter [30] is applied for estimating the polarimetric coherency matrix $[T]$. This allows us to reduce the effects of the speckle noise on the coherency matrix and on the POLSAR features. Fig. 5-(a) presents the color composition of the diagonal elements of the $[T]$ matrix. The Forbes bands phenomenon can be noticed. It corresponds to the pattern visible in the summer SPOT optical image illustrated in Fig. 5-(b).

In the case of optical images, the amount of cryoconites is revealed by a change in the reflectance at the glacier surface. However, with an active fully polarimetric L-band SAR, the interaction between the electromagnetic wave and the clean/dirty ice of the glacier is still difficult to interpret. Firstly, it is important to notice that the presence of cryoconites is not directly related to the backscattering properties, hence the size of the mineral dust is much smaller than the SAR wavelength (approximately 20 cm).

Secondly, as SAR intensity images are affected by the local slope of the target area [43], the presence of terraces influences the radar backscattering signature. Despite that, the strong variations revealed by Fig. 5-(a) cannot entirely be explained by the local slope variations. Fig. 6-(b) presents a spatial profile of the local slope over two consecutive Forbes bands, computed form a 2-meter resolution Digital Terrain Model (DTM[1]) illustrated in Fig. 6-(a). Indeed, the local slope varies within a range of about 10^0.

[Figure 6 about here.]

---

[1] A detailed description of the DTM can be found in [2]

Up to now, the evolution of the SAR backscattering properties along the Forbes bands is unknown. The IFR analysis of Cloude and Pottier attributes should provide information on the dominant scattering mechanisms and allow us to derive a classification of the Forbes bands.

4.2 POLSAR attribute fusion

Fig. 7 shows the POLSAR attributes obtained by applying the Cloude and Pottier decomposition on the IDAN estimated master coherency matrix [diagonal elements illustrated in Fig. 5-(a)]. Among the three parameters presented in Sect. 2, the most discriminating, with respect to Forbes bands phenomenon, are the entropy [Fig. 7-(a)] and the mean α angle [Fig. 7-(b)]. On the contrary, a direct interpretation of the anisotropy [Fig. 7-(c)] is rather difficult as this attribute exhibits no specific spatial information for subjective visual assessment.

[Figure 7 about here.]

[Figure 8 about here.]

The 2-D histograms of the three POLSAR attributes are presented in Fig. 8-(a),(b),(c). A first interpretation can be performed by partitioning of the 2D space defined by each pair of POLSAR attributes [24] as illustrated in Fig. 8-(d),(e),(f). The conventional code of colors proposed by POLSARpro software [8] is used: red for double bounce, green for volume scattering and blue for single bounce. In all cases, the luminance is proportional to the entropy value, meaning that the brighter the color, the higher the mixture of the three backscattering mechanisms. The $H - \alpha$ and $A - \alpha$ histograms [Fig. 8-(a),(c)] reveal a high entropy and a medium α angle: the cloud of points is clustered mainly around the border between the single bounce and volume scattering. This is in accordance with the $H - \alpha - A$ parameters derived for the Fiescherhorn temperate glacier at L band [44].

Once the three POLSAR attributes are computed, the training data set has to be defined. Individual masks have been drawn in the composed-color image made of the 3 intensities in the Pauli basis (see Fig. 5-(a)) in which the Forbes band pattern appears as a periodical color variation. This variation allows to visually detect the presence of two “classes” which create this pattern. For each class, 3 parts located in the upper, middle and lower part of the Tacul glacier have been by manually selected in order to provide examples which include possible attribute variability along the glacier.

The results obtained by the IFR classification with the initial or refined training sets, using two attributes, $H - \alpha$, and 3 attributes, $H - \alpha - A$, are illustrated in Fig. 9. A quantitative assessment of the results is presented in Tables 2 and 3: “pseudo confusion matrices” provide the number of pixels of the initial training set which are classified in each class, in the mixture class or unclassified (reject class).

The visual analysis of the different classifications shows the influence of the training set refinement: with the initial training set, a large proportion of the glacier is classified in the mixture class (cyan) whereas the refined data set reduces the ambiguity between the two classes and allows the green class to appear more clearly. This result is numerically confirmed by the confusion matrix: after refinement, about 60% of the pixels are correctly classified and 40% remain in the mixture class whereas the number of miss classified or unclassified pixels is below 1%. Despite being visually less sensitive to the Forbes bands than the H and α attributes, the anisotropy attribute slightly improves the classification results in both cases.

[Figure 9 about here.]

[Table 2 about here.]

[Table 3 about here.]

[Figure 10 about here.]

The 2D $H-\alpha$ plots from Fig. 10 illustrate the distribution of the training sets selected for the two classes and the polygons derived by the IFR system. One can observe that a simple definition of the convex hull of the point clouds is not sufficient, the initially derived rules from Fig. 10-(a) being too relaxed. By applying the refined IFR analysis, which takes the actual morphology of the clouds of points into account, the obtained fuzzy rules are more conservative and describe more accurately the class prototypes [Fig. 10-(b)].

From the 2 polygons illustrated in Fig. 10-(b), 2 rules have been constructed. Each rule represents a class by a collection of constraints which appear in the premise (see Eq. 13). Each constraint can be seen as a $H-\alpha$ gradual rule: **"The more H is F_1, the more α is F_2"**. An example of such rule is given in Fig. 11 for each class. For the class 2 (blue cluster in Fig. 10-(b)), the rectangular envelop of the polygon defines the closed domain $[0.51, 0.83] \times [26°, 42.9°]$ used for the gradual rule computation (see algorithm 1). The reading of this rule is represented by the dashed line of Fig. 11-(a): when the entropy $H = 0.6$, α has to be in the interval $[26°, 52.3°]$. For the class 1 (red cluster in Fig. 10-(b)), a similar reading of the gradual rule given in Fig. 11-(b) leads to the interval $[20°, 34.3°]$. According to these two analyzed rules, for an entropy level $H = 0.6$, the ambiguity interval for α is $[26°, 34.3°]$.

[Figure 11 about here.]

The four classes observed in Fig. 9-(a) are:

- **Class 1**: the green class corresponds to the green masks [Fig. 5] and to the red cluster form Fig. 10;
- **Class 2**: the blue class corresponds to the blue masks [Fig. 5] and to the blue cluster from Fig. 10;
- **Class 3**: the cyan class to the mixture of the two classes;
- **Class 4**: the black class to undecided regions.

One way to identify **Class 1** and **Class 2** is to measure their sizes onto a longitudinal profile of the glacier. As it is well-known that the clean ice regions are wider than the dirty ones [42], the class assignment leads to the following associations: **Class 1 -** dirty ice and **Class 2 -** clean ice.

In order to interpret the classification results, frontiers defined by Cloude and Pottier are superposed on the 2D plots from Fig. 10. The physical interpretation of the H and α parameters leads to the identification of the dominant mechanism as single bounce (surface backscattering) over the Tacul glacier. However, although the single bounce mechanism dominates, the presence of volume backscattering can also be observed. Indeed, if the dirty ice class belongs completely to the single bounce class, the clean ice class exhibits a tendency to reach the volume backscattering dominant mechanism (higher entropy and α values). This can be directly linked to effects produced by the presence/absence of cryoconites. The mineral dust particles lower the temperature of ice fusion and thus the ice water equivalent is increasing for the dirty ice class. One immediate consequence on the interaction between the radar wave and the glacier ice is that the penetration depth is decreasing. On the contrary, the clean ice class reveal smaller ice water equivalent, hence higher penetration depths. In other words smaller penetration depths explain an increase in the presence of the single bounce mechanism (dirty ice), while higher penetration depths induce an increase in the presence of volume backscattering (clean ice). This conclusion is the first experimental validation of the hypothesis initially proposed by Guy at al. [42] and discussed later on by Rémy and Testut [41], which link the Forbes bands phenomenon to variations in the ice fusion process.

5 Conclusions and perspectives

This paper has proposed a new information fusion system based on implicative fuzzy rules, and its application to the analysis of POLSAR features. The proposed method allows to perform supervised classification by analyzing the training set clusters in the different 2D feature spaces resulting from the different attributes pairs. The experimental results were presented on a real POLSAR data set acquired by the airborne E-SAR system over temperate glaciers in the Alps.

The results obtained on the Tacul glacier, show the benefits of using polarimetric SAR remote sensing data to extract geophysical knowledge on the highly complex glacier surfaces. The IFR analysis allows the interpretation of the POLSAR attributes (e.g. polarimetric entropy, mean α angle) with respect to the glaciological models existing in the literature. In the case of the Tacul glacier, several conclusions regarding the mixture ice-cryoconite were drawn. The observed interactions between the electromagnetic waves and the glacier body are encouraging in terms of validating glaciologists' hypothesis about the origin of the Forbes bands phenomenon.

From the methodological point of view, the use of implicative rules provides a solution to the embedding of constraints into a fuzzy rule-based system. The interest of this approach is potentially manifold: easy interfacing with knowledge-based fuzzy systems and existing development tools, possibility of extending the approach to the classification of fuzzy points, specifying queries in data mining applications, ... The proposed representation could be improved by using fuzzy gradual rules as introduced in [37]. It would enable us to distinguish typical members of a class, which remain in subareas with high membership degrees, from borderline members, which go through subareas with smaller membership degrees. The perspectives also include the handling of nonlinear constraints and the simplification of a set of implicative rules. Indeed, the redundancy of a collection of global constraints could be reduced to improve the rules interpretability.

Acknowledgment

The authors wish to thank the French Research Agency for supporting this work performed in the MEGATOR project (www.lis.inpg.fr/megator), and the Microwaves and Radar Institute DLR-HR for the E-SAR images. They would like to express their gratitude to all participants of the experiment performed in October 2006: I. Hajnsek, R. Horn, M. Keller, C. Andres (DLR-HR Oberpfaffenhofen); P. Grussenmeyer, M. Koehl, E. Smigiel, S. Guillemin, T. Landes (MAP-PAGE, CNRS-INSA Strasbourg); J.-M. Vanpé, L. Ott, L. Bombrun (GIPSA-lab, CNRS-INP Grenoble); Ph. Bolon (LISTIC, Université de Savoie); G. Lehureau, L. Denis, F. Tupin, J.-M. Nicolas (TSI, CNRS-GET Télécom Paris); N. Longepe, L. Ferro-Famil (IETR, CNRS-Université de Rennes 1); J. Deparis (LGIT, CNRS-INP Grenoble); L. Moreau (EDYTEM, CNRS-Université de Savoie); R. Lecluse.

References

[1] J. Vallot. Expérience sur la marche et la variation de la Mer-de-Glace. *Annales de l'Observatoire Météorologique, Physique et Glaciaire du Mont-Blanc*, 4:35–157, 1900.

[2] E. Trouvé, G. Vasile, M. Gay, L. Bombrun, P. Grussenmeyer, T. Landes, J. M. Nicolas, P. Bolon, I. Petillot, A. Julea, L. Valet, J. Chanussot, and M. Koehl. Combining airborne photographs and spaceborne SAR data to monitor temperate glaciers. Potentials and limits. *IEEE Transactions on Geoscience and Remote Sensing*, 45(4):905–924, 2007.

[3] A. Julea, G. Vasile, I. Petillot, E. Trouvé, M. Gay, J. M. Nicolas, and P. Bolon. Simulation of SAR images and radar coding of georeferenced information for temperate glacier monitoring. In *Proc. OPTIM, Brasov, Romania*, volume 4, pages 175–180, 2006.

[4] G. Vasile, F. Pascal, J. P. Ovarlez, P. Formont, and M. Gay. Optimal parameter estimation in heterogeneous clutter for high resolution polarimetric SAR data. *IEEE Geoscience and Remote Sensing Letters*, 8(6):1046–1050, 2011.

[5] A. Anghel, G. Vasile, C. Cacoveanu, C. Ioana, and S. Ciochina. Short-range wideband FMCW radar for millimetric displacement measurements. *IEEE Transactions on Geoscience and Remote Sensing*, 52(9):5633–5642, 2014.

[6] N. Besic, G. Vasile, J. P. Dedieu, J. Chanussot, and S. Stankovic. Stochastic approach in wet snow detection using multitemporal SAR data. *IEEE Geoscience and Remote Sensing Letters*, 12(2):244–248, 2015.

[7] E. Berthier, H. Vadon, D. Baratoux, Y. Arnaud, C. Vincent, K. L. Feigl, F. Rémy, and B. Legrésy. Mountain glacier surface motion derived from satellite optical imagery. *Remote Sensing of Environment*, 95(1):14–28, 2005.

[8] E. Pottier, L. Ferro-Famil, S. Allain, S. Cloude, I. Hajnsek, K. Papathanassiou, A. Moreira, M. Williams, T. Pearson, and Y. Desnos. An overview of the PolSARpro v2.0 software. The educational toolbox for polarimetric and interferometric polarimetric SAR data processing. In *POLinSAR 2007 Workshop, ESA, Franscati, Italy*, pages CD–ROM, 2007.

[9] S.R. Cloude and E. Pottier. An entropy based classification scheme for land applications of polarimetric SAR. *IEEE Transactions on Geoscience and Remote Sensing*, 35(1):68–78, 1997.

[10] S. R. Cloude. Group theory and polarization algebra. *OPTIK*, 75(1):26–36, 1986.

[11] J. R. Huynen. Measurement of the target scattering matrix. *Proc. IEEE*, 53:936–946, 1965.

[12] W. Holm and R. M. Barnes. On radar polarization mixed target state decomposition. In *IEEE 1988 National Radar Conf., Ann Arbor, USA*, pages 249–254, 1988.

[13] E. Krogager. New decomposition of the radar target scattering matrix. *Electron. Lett.*, 26(18):1525–1527, 1990.

[14] W. L. Cameron and L. K. Leung. Feature motivated polarization scattering matrix decomposition. In *IEEE Int. Radar Conf., Arlington, USA*, pages 549–557, 1990.

[15] A. Freeman and S. L. Durden. A three-component scattering model for polarimetric SAR data. *IEEE Transactions on Geoscience and Remote Sensing*, 36(3):963–973, 1998.

[16] R. Touzi. Target scattering decomposition in terms of roll-invariant target parameters. *IEEE Transactions on Geoscience and Remote Sensing*, 45(1):73–84, 2007.

[17] J. S. Lee and M. R. Grunes. Polarimetric SAR speckle filtering and terrain classification - An overview. *Information Processing for Remote Sensing, C. H. Chen, Ed, Singapore: World Scientific*, pages 113–138, 1999.

[18] R. Touzi, W. M. Boerner, J. S. Lee, and E. Lueneburg. A review of polarimetry in the context of synthetic apperture radar: concepts and information extraction. *Canadian Journal of Remote Sensing*, 30(3):380–407, 2004.

[19] J. J. vanZyl. Unsupervised classification of scattering mechanisms using radar polarimetry data. *IEEE Transactions on Geoscience and Remote Sensing*, 35(1):36–45, 1989.

[20] Y. Dong, A. K. Milne, and B. C. Forster. Segmentation and classification of vegetated areas using polarimetric SAR image data. *IEEE Transactions on Geoscience and Remote Sensing*, 39(2):321–329, 2001.

[21] C. T. Chen, K. S. Chen, and J. S. Lee. The use of fully polarimetric information for the fuzzy neural classification of SAR images. *IEEE Transactions on Geoscience and Remote Sensing*, 41(9):2089–2100, 2003.

[22] J. M. Beaulieu and R. Touzi. Segmentation of textured polarimetric SAR scenes by likelihood approximation. *IEEE Transactions on Geoscience and Remote Sensing*, 42(10):2063–2072, 2004.

[23] J. S. Lee, M. R. Grunes, T. L. Ainsworth, D. Li-Jen, D. L. Schuler, and S. R. Cloude. Unsupervised classification using polarimetric decomposition and the complex Wishart classifier. *IEEE Transactions on Geoscience and Remote Sensing*, 37(5):2249–2258, 1999.

[24] L. Ferro-Famil, E. Pottier, and J. S. Lee. Unsupervised classification of multifrequency and fully polarimetric SAR images based on the H/A/Alpha-Wishart classifier. *IEEE Transactions on Geoscience and Remote Sensing*, 39(11):2332–2342, 2001.

[25] J. S. Lee, M. R. Grunes, E. Pottier, and L. Ferro-Famil. Unsupervised terrain classification preserving polarimetric scattering characteristics. *IEEE Transactions on Geoscience and Remote Sensing*, 42(4):722–731, 2004.

[26] P. R. Kersten, J. S. Lee, and T. L. Ainsworth. Unsupervised classification of polarimetric synthetic aperture radar images using fuzzy clustering and EM clustering. *IEEE Transactions on Geoscience and Remote Sensing*, 43(3):519–527, 2005.

[27] T. Landes, M. Gay, E. Trouve, J. M. Nicolas, L. Bombrun, G. Vasile, and I. Hajnsek. Monitoring temperate glaciers by high resolution Pol-InSAR data: first analysis of Argentiere E-SAR acquisitions and in-situ measurements. In *IEEE Geoscience and Remote Sensing Symposium Proceedings, Barcelona, Spain*, pages 184–187, 2007.

[28] J. D. Forbes. *Travels through the Alps of Savoy and other parts of the Pennin chain with observations on the phenomena of Glaciers (second ed.).* Adam & Charles Black, Edinburgh, 1845.

[29] S. R. Cloude and K. P. Papathanassiou. Polarimetric SAR interferometry. *IEEE Transactions on Geoscience and Remote Sensing*, 36(5):1551–1565, 1998.

[30] G. Vasile, E. Trouvé, J. S. Lee, and V. Buzuloiu. Intensity-Driven-Adaptive-Neighborhood Technique for polarimetric and interferometric SAR parameters estimation. *IEEE Transactions on Geoscience and Remote Sensing*, 44(5):1609–1621, 2006.

[31] H. Yu, J. Han, and K. C. C. Chang. PEBL: web page classification without negative examples. *IEEE Transactions on Knowledge and Data Engineering*, 16(1):70–81, 2004.

[32] F. Hoffmann. Combining boosting and evolutionary algorithms for learning of fuzzy classification rules. *Fuzzy Sets and Systems*, 141:45–58, 2004.

[33] Y. C. Hu and G. H. Tzeng. Elicitation of classification rules by fuzzy data mining. *Engineering Applications of Artificial Intelligence*, 16:709–716, 2003.

[34] H. Ishibuchi and T. Nakashima. Effect of rule weights in fuzzy rule-based classification systems. *IEEE Transactions on Fuzzy Systems*, 9(4):506–515, 2001.

[35] H. Ishibuchi and T. Yamamoto. Fuzzy rule selection by multi-objective genetic local search algorithms and rule evaluation measures in data mining. *Fuzzy Sets and Systems*, 141:59–88, 2004.

[36] D. Dubois and H. Prade. Gradual inference rules in approximate reasoning. *Information Sciences*, 61(1-2):103–122, 1992.

[37] S. Galichet, D. Dubois, and H. Prade. Imprecise specification of ill-known functions using gradual rules. *International Journal of Approximate Reasoning*, 35(3):205–222, 2004.

[38] L. Darlea, S. Galichet, and L. Valet. Classification rules with premise expressed as the conjunction of implications. In *11th Int. Fuzzy Systems Association World Congress (IFSA'2005), Beijing, China*, pages 1040–1045, 2005.

[39] L. Lliboutry and L. Reynaud. "Global dynamics" of a temperate valley glacier, Mer de Glace, and past velocities deduced from Forbes'bands. *Journal of Glaciology*, 27(96):207–226, 1981.

[40] H. vonHelmholtz. Ice and glaciers. *Scientific Papers. The Harvard Classics. New York: P. F. Collier & Son*, 30, 2001.

[41] F. Rémy and L. Testut. But how a glacier can flow? Historical outlines. *C. R. Geoscience*, 338:368–385, 2006.

[42] B. Guy, M. Daigneault, and G. Thomas. Reflections on the formation of Forbes ogives: the instability of fusion of dirty ice. *C. R. Geoscience*, 334:10611070, 2002.

[43] G. Vasile, I. Petillot, A. Julea, E. Trouvé, P. Bolon, L. Bombrun, M. Gay, T. Landes, P. Grussenmeyer, and J. M. Nicolas. High resolution SAR interferometry: influence of local topography in the context of glacier monitoring. In *IEEE Geoscience and Remote Sensing Symposium, Denver, USA*, pages 4008–4011, 2006.

[44] O. Stebler, A. Schwerzmann, M. Luthi, E. Meier, and D. Nuesch. Pol-InSAR observations from an Alpine glacier in the cold infiltration zone at L- and P-band. *IEEE Geoscience and Remote Sensing Letters*, 2(3):557–361, 2005.

List of Figures

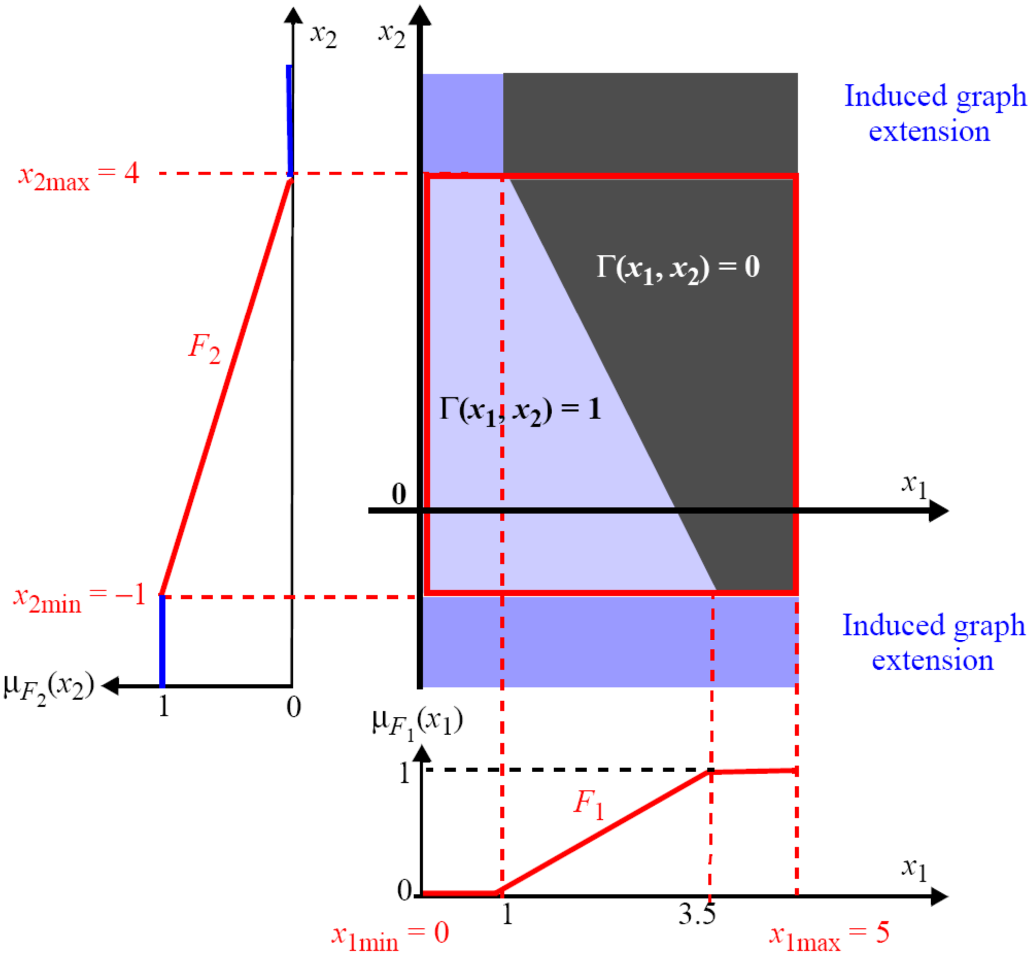

Figure 1: Graph of the fuzzy gradual rule "**If** x_1 **is** F_1 **then** x_2 **is** F_2".

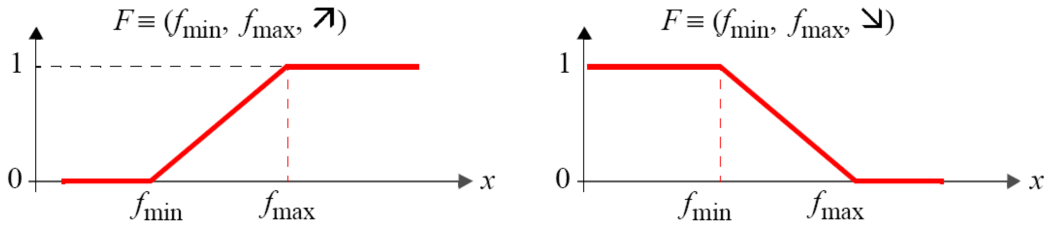

Figure 2: Ramp-shaped membership functions.

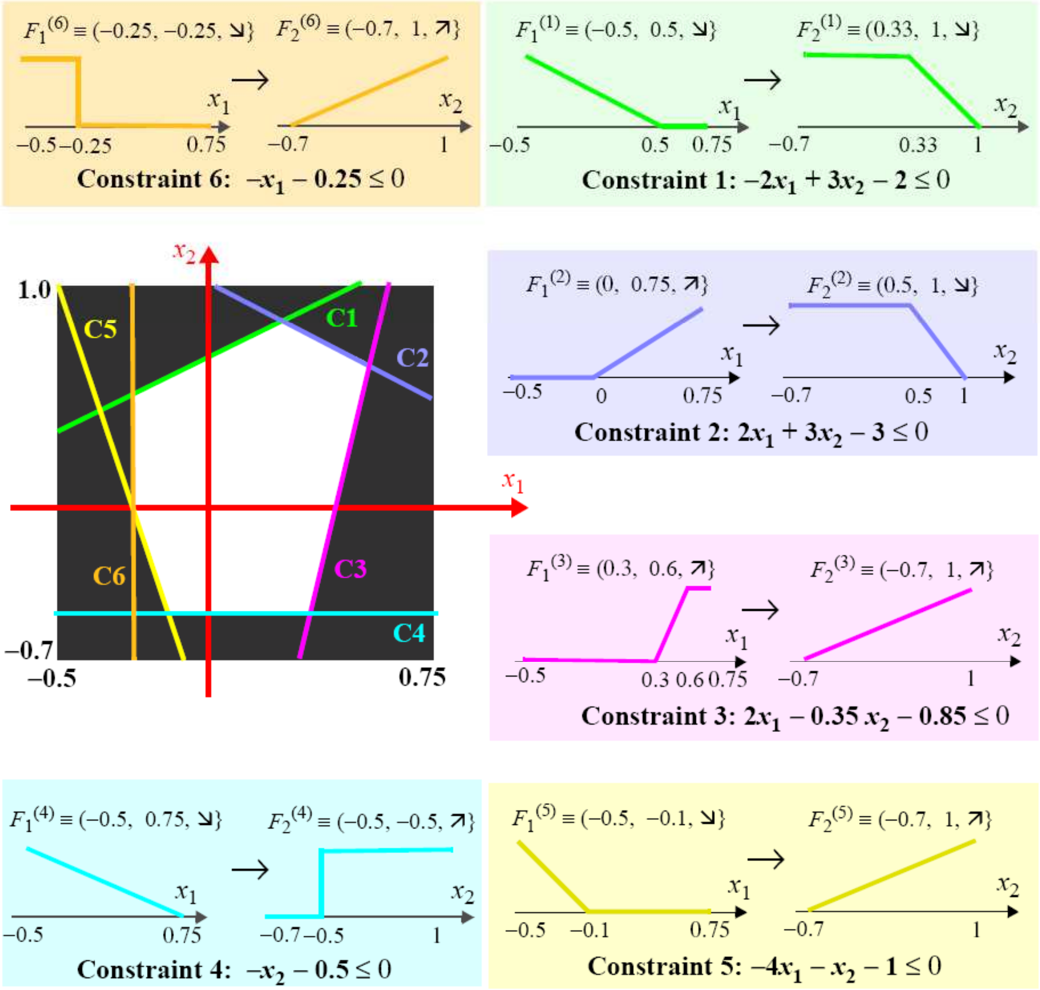

Figure 3: Representation of a 6-side polygon by an implication-based fuzzy rule.

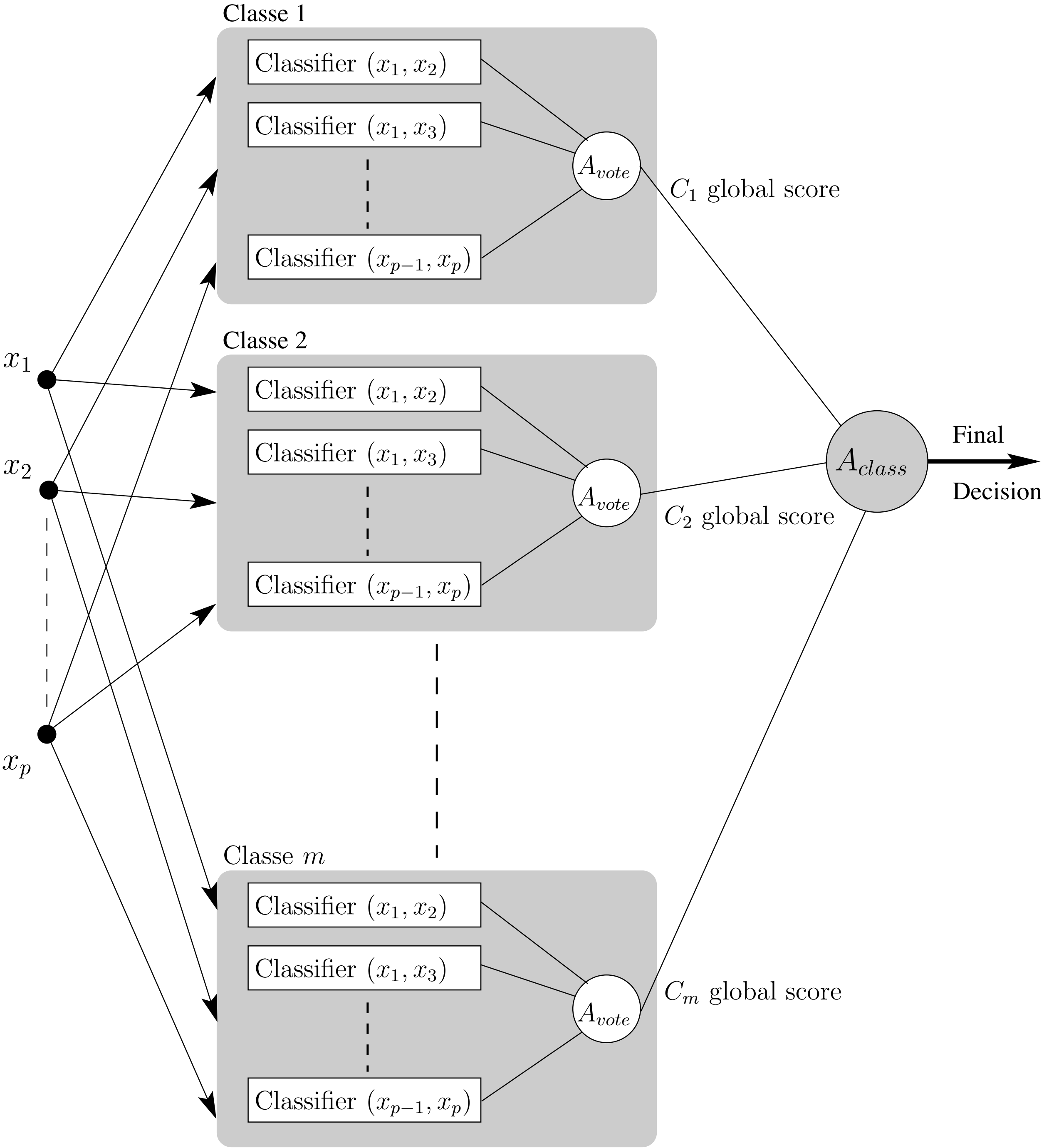

Figure 4: Multi attributes, multi classes classification

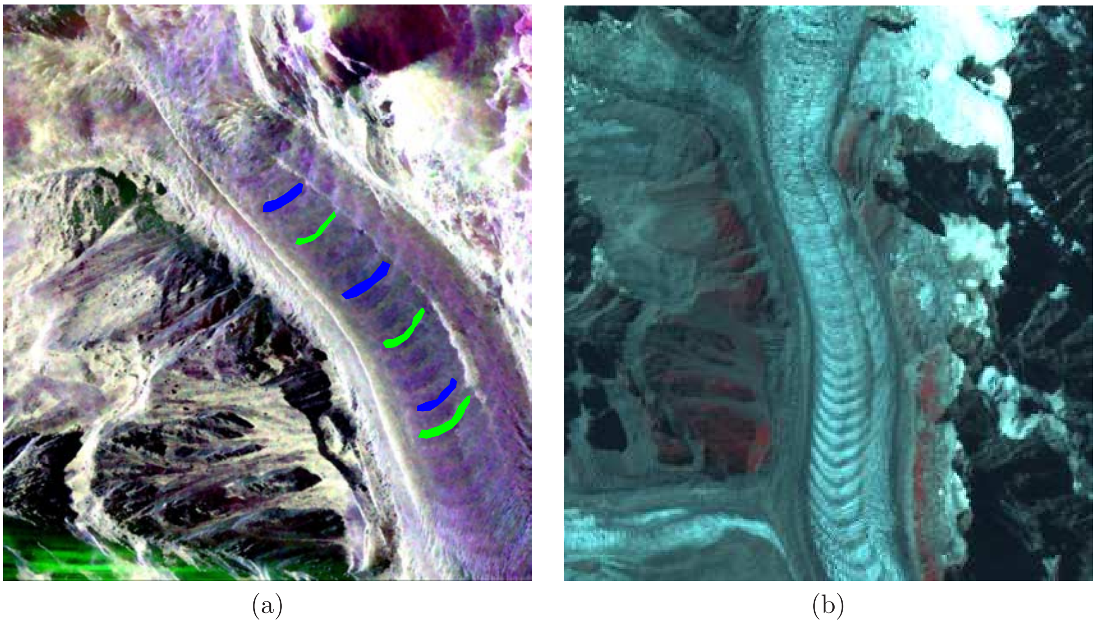

Figure 5: Tacul glacier: (a) E-SAR L band image, October 2006, colored composition of the IDAN estimated $[T]$ diagonal terms HH-VV, 2HV, HH+VV (1205×1312 pixels). The masks used in the selection of the training sets are represented in blue and green. (b) multi-spectral SPOT–5 image, August 2005.

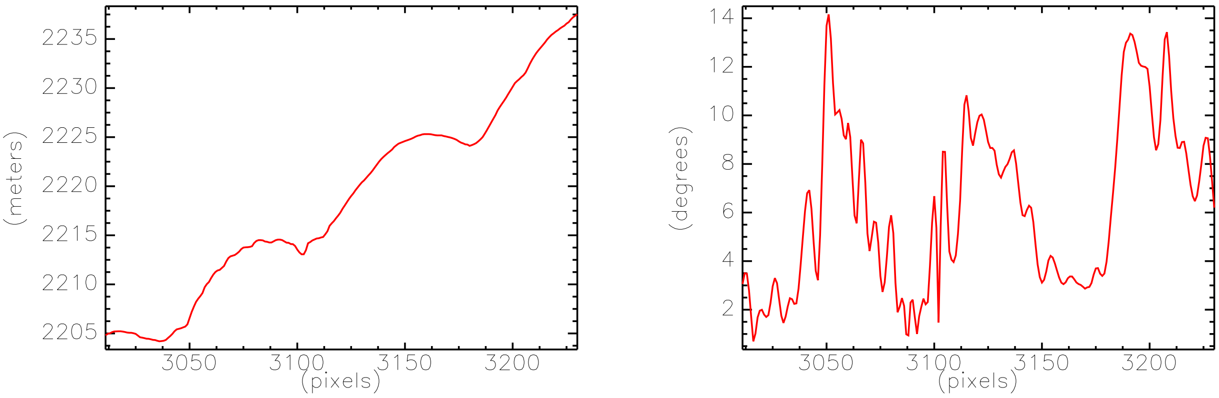

(a)

(b)

Figure 6: Spatial profiles, Tacul glacier, 2-meter resolution DTM: (a) elevation profile, (b) local slope profile.

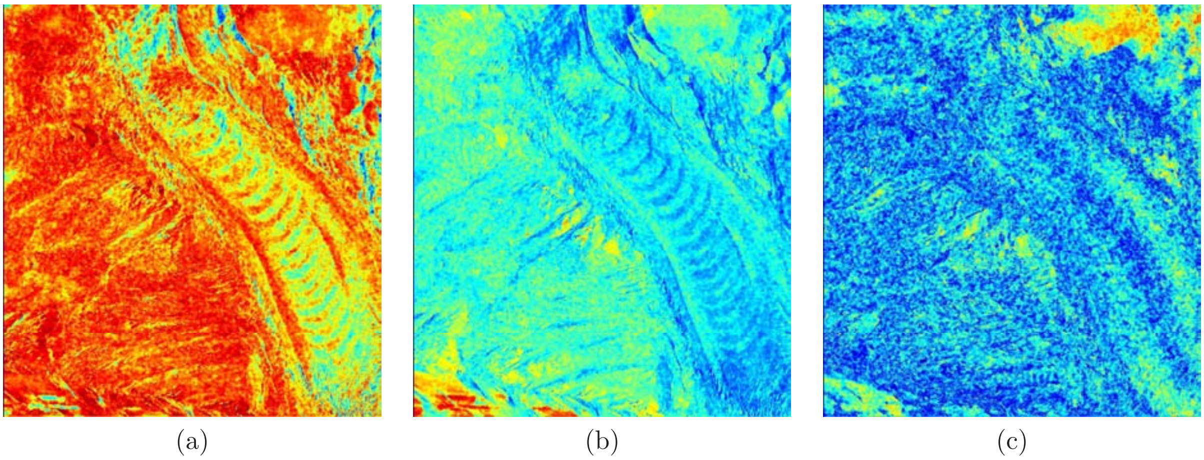
(a) (b) (c)

Figure 7: Cloude and Pottier decomposition, E-SAR data, Tacul glacier, L band, [1205 × 1312 pixels]: (a) entropy, (b) mean α angle, (c) anisotropy.

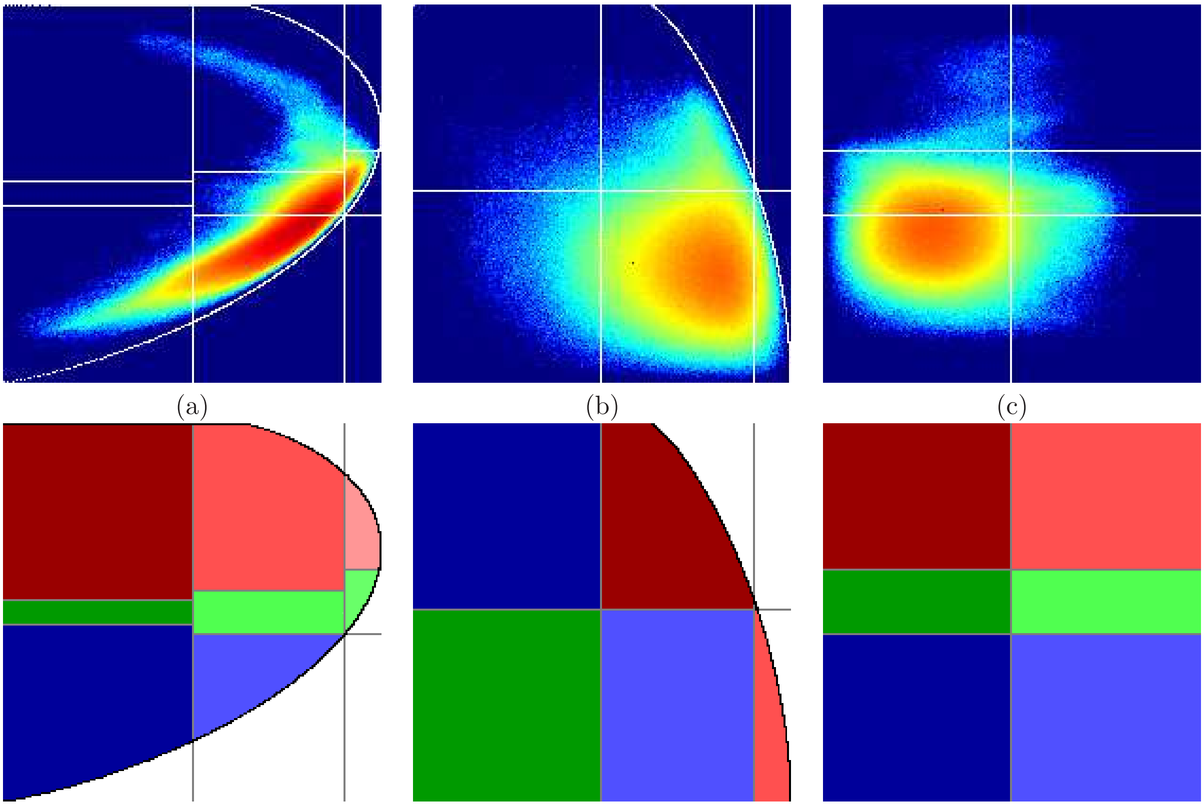

(a) (b) (c)

(d) (e) (f)

Figure 8: 2D histogrammes of POLSAR attributes, E-SAR data, Tacul glacier, L band: (a) $H-\alpha$ plane, (b) $H-A$ plane, (c) $A-\alpha$ plane. Crisp partition of the $H/\alpha/A$ space in 3 main classes (double bounce, volume scattering, single bounce): (d) $H-\alpha$, (e) $H-A$, (f) $A-\alpha$.

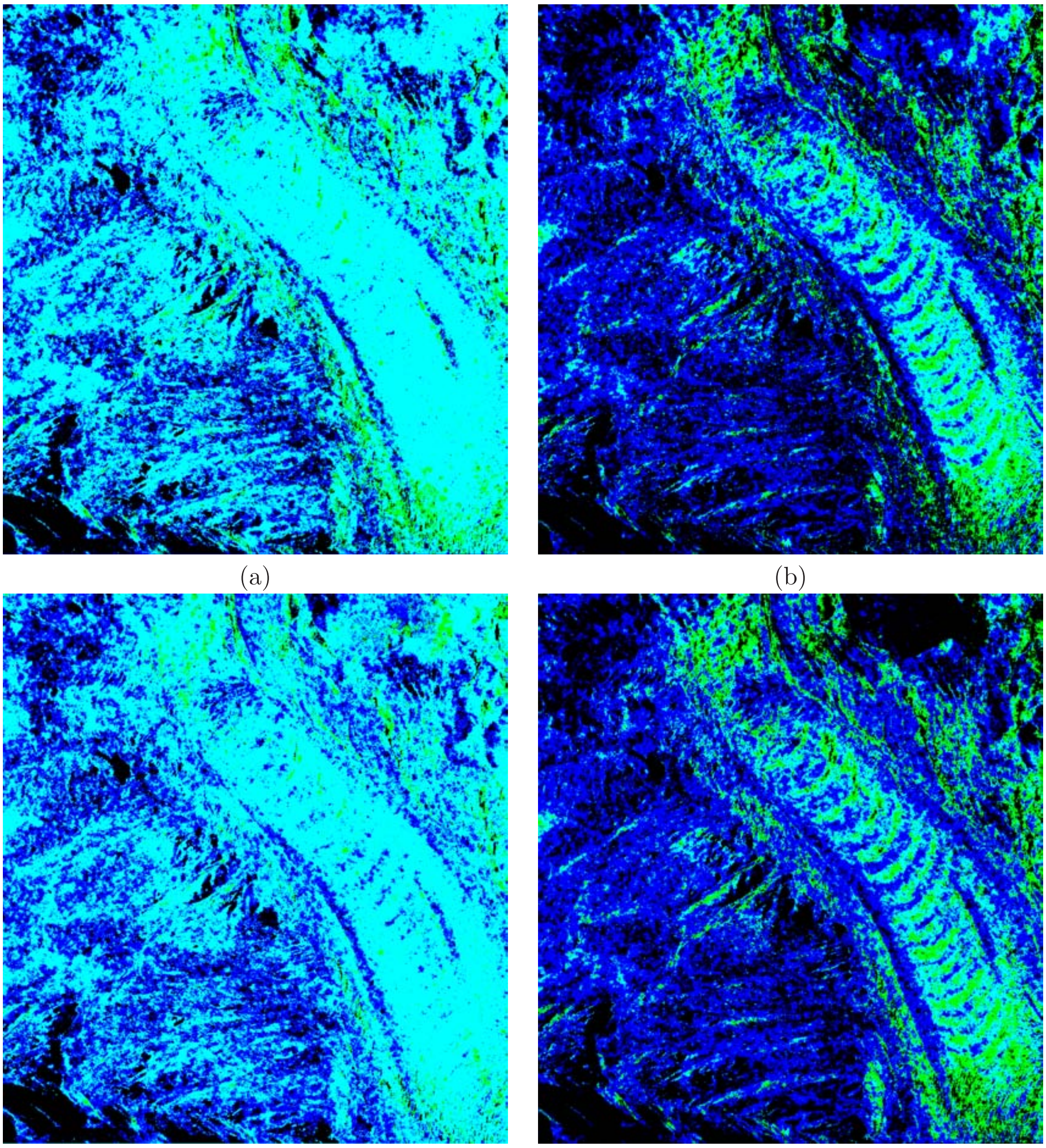

(a) (b)

(c) (d)

Figure 9: Classification results, E-SAR data, Tacul glacier, L band, [1205 × 1312 pixels]. First line: IFR classification in $H-\alpha$ space with (a) the initial training set, (b) the refined training set. Second line: IFR classification in $H-\alpha-A$ space with: (c) the initial training set, (d) the refined training set. Blue and green colors correspond to the two trained classes, cyan to the mixture class and black to unclassified pixels (reject).

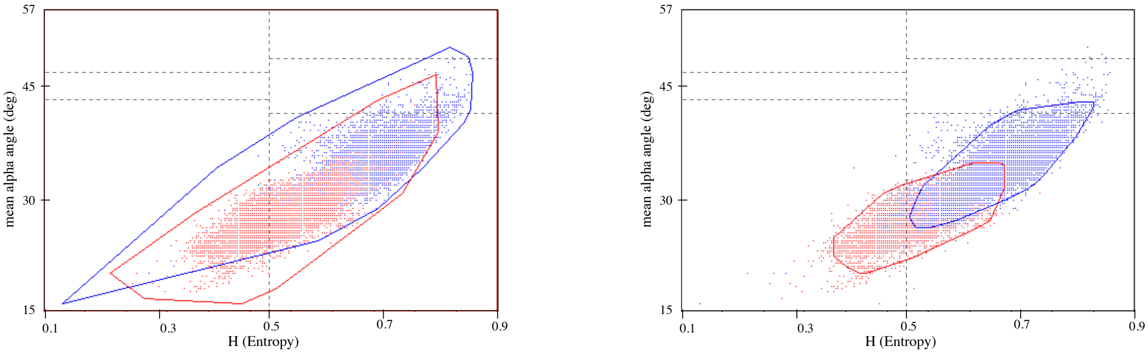

(a) (b)

Figure 10: Rules of the IFR classification in $H - \alpha$ space, E-SAR data, Tacul glacier, L band: (a) initial rules, (b) refined rules.

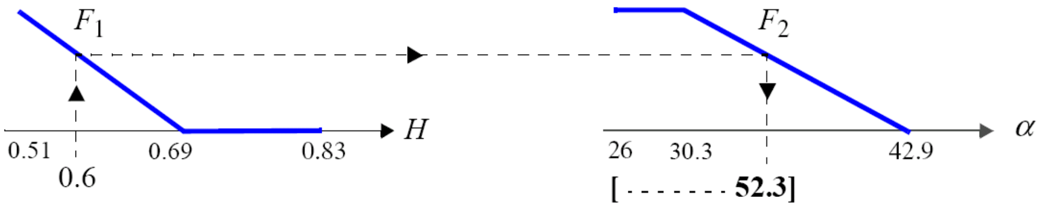

(a) Class 2

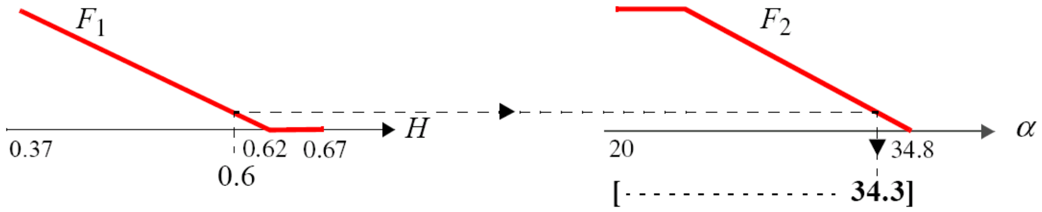

(b) Class 1

Figure 11: Examples of gradual rules build from the refined training set

List of Tables

Table 1: Airborne SAR data acquired over the test area.

Agency	DLR-HR
campaign	MEGATOR
date	2006.10.10
sensor	E-SAR
test site	Chamonix Mont-Blanc
band	L
polarization	HH, VV, XX
SLC range sampling (m)	1.5
SLC azimuth sampling (m)	0.45
altitude above MSL (m)	6040.48

Table 2: Confusion matrix for the IFR classification in $H-\alpha$ space with the initial (left) or refined (right) training sets

C1	C2	C1 and C2	Not classified
158	0	5941	0
0	215	6739	0

C1	C2	C1 and C2	Not classified
3267	77	2585	170
137	3624	2924	269

Table 3: Confusion matrix for the IFR classification in $H - \alpha - A$ space with the initial (left) or refined (right) training sets

C1	C2	C1 and C2	Not classified
185	0	5914	0
0	1133	5821	0

C1	C2	C1 and C2	Not classified
3418	137	2410	134
157	4312	2281	204